

Monitoring Melanoma Responses to STING Agonism and Focused Ultrasound Thermal Ablation Using Microneedles and Ultrasensitive Single Molecule Arrays

Daniel Dahis, Michelle Z. Dion, Alexander M. Cryer, Pere Dosta, Tal Gilboa, Mariana Alonso, Michael Lewandowski, Núria Puigmal, Gonzalo Muñoz Taboada, Haim Azhari, Rushdy Ahmad, David R. Walt, and Natalie Artzi*

Real-time monitoring of immune state and response to therapy can provide a means to stratify patients and increase the number of responders who will benefit from approved and emerging immunotherapies. The accessibility of immune cells in the skin provides an opportunity for local immune modulation as well as for noninvasive sampling of disease biomarkers in the skin interstitial fluid (ISF). Here, a monitoring strategy for melanoma immunotherapy is investigated by longitudinal sampling of biomarkers in the skin ISF using Hyaluronic acid (HA)-based microneedles (MNs). Focused ultrasound ablation and delivery of nanoparticulate stimulator of interferon genes agonist are used as model immunotherapies. It is shown that this combination therapy induces potent inflammatory responses in a melanoma mouse model, promoting tumor elimination and immune memory formation. Indeed, quantifying soluble, protein-based biomarkers following therapy using conventional immunoassay reveals a pronounced proinflammatory program in the tumor. However, conventional assays fail to detect the low concentration of biomarkers in plasma and in MN-sampled ISF. It is shown that ultrasensitive single molecule arrays (Simoa) effectively detected proinflammatory biomarkers that are upregulated in response to the therapy in MN-sampled ISF, in plasma, and in tumors, supporting the feasibility of monitoring melanoma immunotherapy using MNs.

1. Introduction

Melanoma accounts for more than 60–75% of all skin cancer-related mortality globally,^[1] with rising annual incidence.^[2] Melanoma treatment was substantially improved following the 2011 FDA approval of novel immunotherapeutic drugs such as the checkpoint inhibitors anticytotoxic T-lymphocyte associated protein 4 (aCTLA-4) and antiprogrammed cell death protein 1 (aPD-1),^[3] with numerous cases of tumor remission and long-term survival.^[4,5] However, less than 52% of patients benefit from this class of drugs, potentially due to differences in the composition and phenotype of their immune cells in the tumor microenvironment (TME).^[6,7] Among responders to immunotherapy, resistance can be primary or acquired following an initial response period.^[7] Consequently, there is an acute need for alternative strategies to monitor melanoma responses to therapy.

Existing methods for monitoring melanoma immunotherapy are broadly

D. Dahis, H. Azhari
Technion Institute of Technology
Haifa 320003, Israel
E-mail: dahisdaniel@campus.technion.ac.il

D. Dahis, M. Z. Dion, A. M. Cryer, P. Dosta, N. Puigmal, G. M. Taboada, N. Artzi
Institute for Medical Engineering and Science
Massachusetts Institute of Technology
Cambridge, MA 02139, USA
E-mail: nartzi@bwh.harvard.edu


D. Dahis, M. Z. Dion, A. M. Cryer, P. Dosta, M. Alonso, N. Puigmal, N. Artzi
Brigham and Women's Hospital
Harvard Medical School
Boston, MA 02115, USA

D. Dahis, M. Z. Dion, A. M. Cryer, P. Dosta, T. Gilboa, M. Lewandowski, N. Puigmal, R. Ahmad, D. R. Walt, N. Artzi
Wyss Institute for Biologically-Inspired Engineering
Harvard University
Boston, MA 02115, USA

M. Z. Dion
Harvard-MIT Division of Health Sciences & Technology, Massachusetts
Institute of Technology, Cambridge, MA, USA
Cambridge 02139, United States

T. Gilboa, D. R. Walt
Department of Pathology, Brigham and Women's Hospital
Harvard Medical School Boston
Boston, MA 02115, USA

N. Artzi
Broad Institute of Harvard and MIT
Cambridge, MA 02139, USA

 The ORCID identification number(s) for the author(s) of this article can be found under <https://doi.org/10.1002/adfm.202301659>

DOI: 10.1002/adfm.202301659



designed to predict which patients would benefit from the therapy, or over-time monitoring of tumor responses.^[8] Examples of predictive strategies include measuring checkpoint expression and cellular compositions in tumor biopsies^[9] and circulating biomarkers such as lactate dehydrogenase (LDH^[10]), which is a negative prognostic marker associated with tumor burden.^[11] Direct monitoring of responses to therapy utilize molecular imaging techniques such as positron emission tomography–computed tomography (PET–CT) with 2-deoxy-2-(¹⁸F)fluoro-D-glucose (¹⁸F-FDG) which have been in clinical use for tumor staging and metastasis tracing^[12] with novel preclinical tracers for predicting the response rate.^[13,14] Additionally, the analysis of biomarkers, such as circulating tumor DNA (ctDNA) and tumor cells (CTCs) in the blood (liquid biopsy^[15]) have been proposed for continuous treatment monitoring given its advantageous minimally invasive nature. However, these techniques can be time-consuming and expensive (PET-CT), invasive (biopsy), or lack appropriate sensitivity and specificity (biomarkers in liquid biopsy, such as ctDNA).^[16,17]

Skin interstitial fluid (ISF), is a rich source of local biomarkers that correlate with the ones in plasma.^[18–21] ISF is currently being used for continuous glucose monitoring,^[22,23] and preclinical work has highlighted its potential for revealing features of the tumor microenvironment.^[24,25] Consequently, ISF sampling is a promising localized method for monitoring melanoma tumors. However, ISF sampling is challenging as 70% of the ISF is found in the lower dermis layer.^[26]

Strategies for collecting skin ISF include invasive biopsies,^[27,28] suction blisters,^[20,29,30] microanalysis arrays,^[31,32] and reverse iontophoresis.^[33,34] We and others have proposed using hydrogel-based microneedles (MNs) for skin ISF sampling.^[35–40] MNs are comprised of an array of submillimetric needles that are engineered to allow efficient tissue penetration and high swelling capacity. Hyaluronic acid-based microneedles (HA MNs) are especially attractive as these hydrogels are biocompatible and were shown to achieve high swelling characteristics postapplication, allowing for efficient collection of cells^[39] and other biomarkers present in the ISF, such as proteins.^[36,40] Analyzing cytokines and chemokines in the ISF could provide valuable insights, as these biomolecules are key mediators of immune cell communication in the TME.^[41] However, the ISF volume collected by MNs is low (<3 μ L), and gets further diluted while isolating proteins from it. As a result, there is a need for a sensitive and accurate method for detecting low levels of biomarkers isolated from ISF. Single molecule arrays (Simoa) are a bead-based digital enzyme-linked immunosorbent assay (ELISA), that is capable of detecting low levels (i.e., attomolar/femtomolar concentrations^[42]) of proteins with ultrasensitivity and high accuracy.^[43,44] Hence, we hypothesized that combining MNs for biomarker collection and Simoa for protein quantification could result in an efficient method for monitoring immunotherapy responses.

Focused ultrasound (FUS)-mediated thermal ablation and nanoparticulate stimulator of interferon genes (STING) agonism (CDN NPs) are promising immunotherapies that have been used here as model immune-modulating therapies. These therapies were selected in light of previous studies showing that STING stimulation and thermal ablation therapies induce distinct responses but result in increased tumor cell killing and potent anti-

tumor immune responses when combined.^[45–47] While promising, these reports studied the use of endogenous STING agonists such as cGAMP or c-di-GMP, which are significantly less effective than synthetic cyclic dinucleotides (CDN) analogs, are typically less stable and require higher doses with potential for side effects.^[48] Additionally, previous studies employed invasive heating modalities such as microwave ablation,^[45] or photothermal therapy,^[46,47] which typically reach only a few millimeters within the tissue. FUS is a noninvasive modality that concentrates acoustic waves into a millimetric volume deep inside tissues. Where the beams converge, heat dissipates to the target tissue (e.g., tumor), elevating its temperature to 50–60 °C in a few seconds, promoting instantaneous and subsequent cancer immunogenic cell death (ICD) and coagulative necrosis.^[49–53] FUS sonication has gained particular interest in the last decades because of its noninvasive and nonionizing nature, highly precise tissue targeting, deep tissue penetration, and ability to target multiple locations of the tumor microenvironment. In parallel, STING agonism is capable of triggering a potent type I interferon (IFN-I)-driven inflammatory response^[54] and has been shown to promote maturation of antigen presenting cells (APCs), enhance the uptake and processing of antigens, and elicit the release of proinflammatory cytokines, while polarizing myeloid-derived suppressor cells to become antitumorogenic.^[55–57] STING agonists such as cyclic dinucleotides (CDN) have been investigated preclinically^[56,58–60] and clinically (NCT03172936, NCT04144140) in the context of melanoma. However, the chemical properties of CDNs, including their hydrophilicity and negative charge, prevent CDNs from readily crossing the cell membrane into the cytoplasm of APCs, thus limiting the potential of this potent innate immune adjuvant.^[61,62] We have previously developed a nanoparticulate form (CDN NPs)^[59] of CDN (ML-317) conjugated to poly(beta-amino esters) polymers via a cathepsin linker, which allows its release in the cell cytosol via enzymatic cleavage.

Here, we studied a novel monitoring strategy employing microneedles and Simoa to detect changes in protein expression in the femtomolar range, using FUS-thermal ablation and nanoparticulate STING agonism model immunotherapies (**Figure 1**). Our results demonstrate that the potent proinflammatory program elicited by the therapies can be sensed by sampling ISF via MNs, which revealed similar profiles with the ones observed in plasma and tumors as measured via ultrasensitive Simoa, suggesting the feasibility of a noninvasive MN-based ISF sampling for melanoma immunotherapy monitoring.

2. Results

The immunogenicity induced by the proposed therapies was studied for each therapy alone and in combination. Particularly, for STING, we leveraged our recently developed CDN NPs that were shown to achieve high CDN conjugation and enzyme-responsive drug release inside immune cells, promoting remarkable antitumor responses in melanoma tumor-bearing mice, enhancing immune cell activation by orders of magnitude compared to free CDN.^[59] CDN NPs were 54.8 \pm 1.1 nm in size and +23.4 mV in surface charge, and were not altered by the heat treatment (**Figure S6**, Supporting Information). The particles were stable for \approx 2 weeks at room temperature with absolute measured

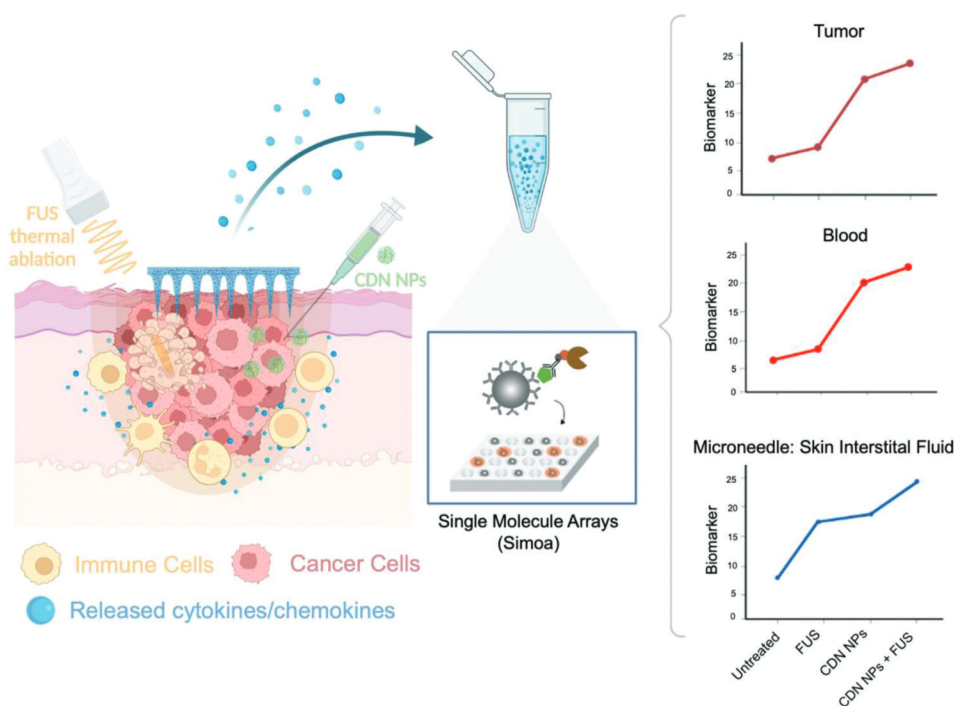


Figure 1. Proposed strategy for monitoring melanoma immunotherapy. Monitoring strategy employing microneedle-based ISF sampling and Simoa quantification: Cytokines/chemokines released by activated immune cells in the TME, which are also present in the ISF, are collected via microneedles applied on top of tumors and analyzed using Simoa. Readings are between tissues and across treatment groups.

size for CDN NPs and heated CDN NPs on day 14 of 141.9 ± 14.2 and 165.5 ± 13.9 nm, respectively (Figure 2C), followed by aggregation over time, which is commonly seen with NPs stored at RT for prolonged periods of time (Figure S6, Supporting Information). To assess the immune activation of CDN NPs, we used the STING-reporter RAW cells, which are murine macrophages genetically modified to report upon STING activation (Figure 2A). These cells, effectively uptake CDN NPs (Figure 2B) and respond by a dose-dependent activation of the interferon regulatory factors (IRF)-pathway (Figure 2C; and Figure S7, Supporting Information), without depicting a reduction in cell viability which was also confirmed by exposing cancer cells to NPs treatment (Figures S6 and S7, Supporting Information). While free CDN was unable to activate RAW cells below 500 nM, CDN NPs (with or without heat) initiated a substantial activation at all concentrations tested with up to 147-fold higher activation than free CDN ([CDN] = 62.5 nM). As macrophages and cancer cells are both present in the tumor microenvironment, we also investigated CDN NPs activation (1 or 10 nM) of RAW cells when in the presence of cancer cells at varied RAW to cancer cell ratios (Figure S8, Supporting Information). We found that at 10 nM CDN NPs concentration the activation of RAW cells was reduced by 31% on average for the majority of cell ratios tested, suggesting that CDN NPs are being uptaken by both RAW cells and B16-F10 cells. We also studied the effect of CDN NPs in the phagocytic activity of bone-marrow derived macrophages (BMDMs) of cancer cells (Figure S9, Supporting Information). Primary cells treated with CDN NPs exhibited 73.8% increased phagocytosis of cancer cells when compared to naïve BMDMs. This effect was similar when primary cells were treated in the presence of ablated cancer cells,

exhibiting 76.1% enhanced phagocytosis to naïve cells when also treated with CDN NPs.

In parallel, we assessed the effects of thermal ablation on melanoma B16-F10 cells in the context of ICD (as measured by the released ATP, high mobility group box-1 (HMGB-1), calreticulin (CRT) expression), and necrosis (as measured via Annexin V, viability dye assay) (Figure 2D). While thermal treatment effectively reduced B16-F10 cell viability to 50% after 24 h (Figure 2E), ATP presence in the supernatant was significantly higher following treatment as a function of thermal dose (0, 15, 30, or 45 s at 60 °C) (Figure 2F), with a similar trend observed for high mobility group box-1 (Figure 2G). Notably, B16-F10 calreticulin expression following 60 s at 60 °C was significantly increased compared to other groups (Figure 2H; and Figure S10, Supporting Information). Annexin V—viability dye assessment of necrosis and apoptosis quantification revealed increased percentages of cancer cells undergoing primary (Figure 2I) and secondary (Figure 2J) necrosis as a function of thermal dose (Figure S11, Supporting Information). Collectively, these results reaffirm the potential of nanoparticulate STING agonism to stimulate a type I interferon response, while thermal ablation serves as an ICD inducer agent.

Given the observed immune-stimulating effects *in vitro*, we next tested the combination of these therapies *in vivo*. Mice were orthotopically implanted with B16-F10 tumors and treated on days 7 and 9 post-tumor inoculation with the combination of CDNs and thermal ablation. The combined treatment was compared to each monotherapy alone or no-treatment control. On both treatment days, animals received an intratumoral injection of CDN NPs, while FUS-mediated thermal ablation was applied to the relevant groups on day 9 (Figure 3A). FUS was applied

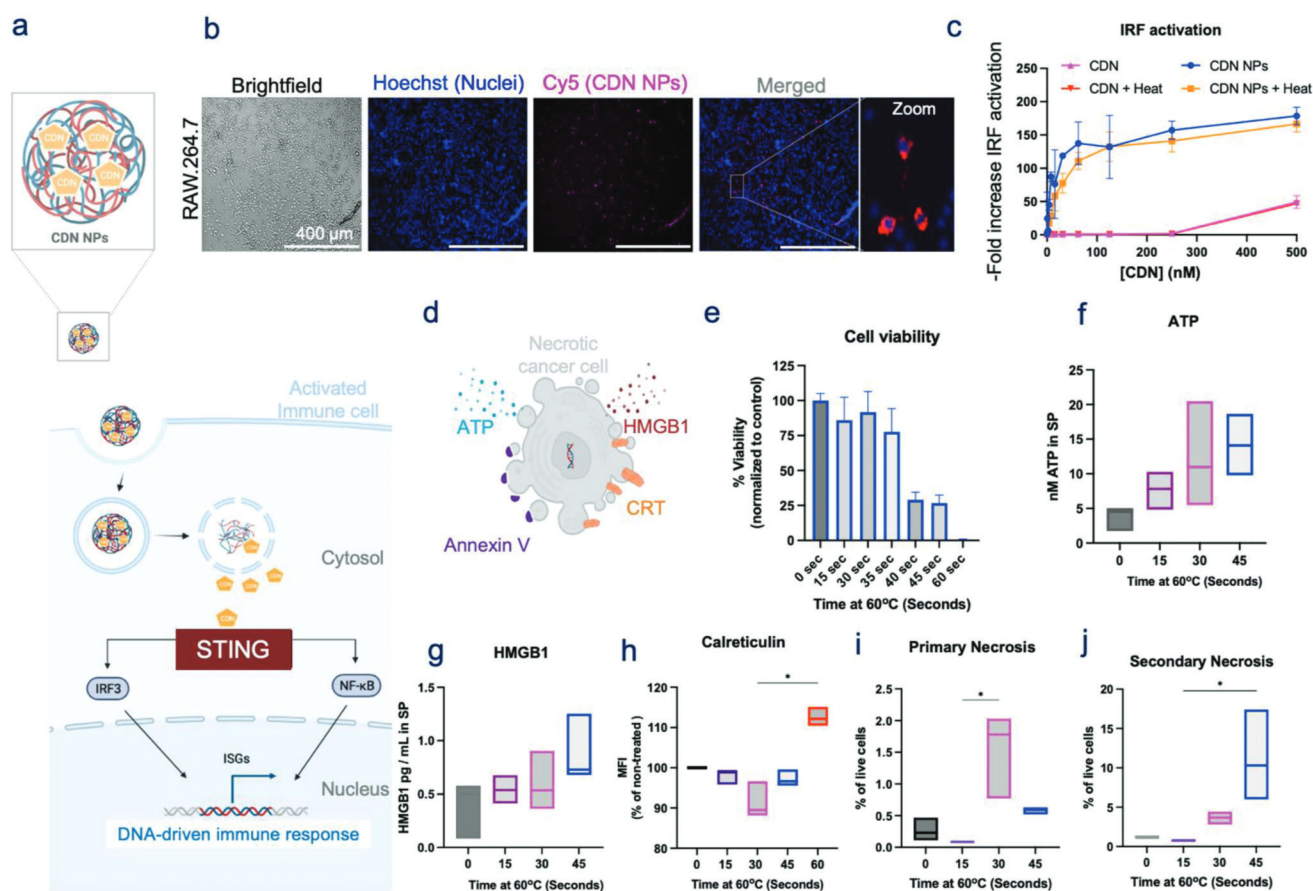


Figure 2. Thermal treatment does not affect CDN NPs stability and induces cancer-cell ICD. A) Schematic illustration depicting the STING activation mechanism of CDN NPs. B) Fluorescent images of internalized CDN NPs (Cy5) in RAW cells. C) RAW cell IRF activation upon CDN or CDN NPs (with/without heat) treatment. D) Schematic of cancer-cell ICD and expression of ATP, HMGB-1 secretion, calreticulin (CRT), and Annexin V E) B16-F10 viability 24 h following heat treatment at 60 °C for different durations. F) Quantification of ATP in the supernatant 24 h post-treatments. G) Quantification of HMGB1 in the supernatant 24 h post-treatments. H) CRT expression using flow cytometry of untreated cancer cells and cells treated for 60 s at 60 °C 24 h post-treatment. I) Primary and J) secondary necrosis assessed via flow cytometry (Annexin V⁻/Fixable viability dye⁺). Data are expressed as mean ± SEM, n = 3.

in 4 × 4 target spots atop tumors where each target was separated by 2 mm. Tumors treated with FUS-mediated thermal ablation reached $T > 50$ °C, measured at the focal spot (Figure S12, Supporting Information). Fluorescence microscopy revealed increased necrosis levels (assessed via H&E and Ki-67) and calreticulin expression in the cells surrounding the ablated region compared to untreated tumors (Figure S13, Supporting Information). The selected CDN dose was 250 ng based on a preliminary study showing robust responses (Figure S14, Supporting Information). Tumor growth curves revealed substantially reduced tumor size for animals with CDN NPs treatment and CDN NPs + FUS ablation, while FUS ablation monotherapy was unable to prevent tumor growth compared to control untreated tumors (Figure 3B,C). Animals treated with the combination treatment exhibited 100% (9/9) survival upon primary challenge, whereas 75% of animals (6/8) treated with CDN NPs-only achieved long-term survival (Figure 3D; CDN NPs treatment with and without ablation are not statistically different). Ablation-only and untreated animals depicted median survival of 20 and 22 days, respectively. Long-term survivors (60 days postprimary challenge) that were rechallenged

with a contralateral tumor depicted comparable levels of tumor rejection (83.3% for CDN NPs only and 77.8% for CDN NPs + ablation; not statistically different) (Figure S14, Supporting Information). Interestingly, the effect of each monotherapy on survival differed; 0/9 animals survived more than 24 days following FUS-thermal ablation alone and 6/8 animals survived more than 60 days for CDN NPs alone. However, the combined treatment increased the survival rate, with 9/9 animals surviving more than 60 days.

We next investigated whether the responses observed in the efficacy study (Figure 3) could be monitored noninvasively. To achieve that, we first devised an in vitro experiment recapitulating the in vivo treatment of day 9, which reflects the recruitment and activation of immune cells to the site of ablation in the hours post treatment.^[67,68] We assessed the effect of coculturing RAW cells with thermally ablated B16-F10 cells and the simultaneous addition of CDN NPs (Figure 4A), and noted that the groups that included B16-F10 cells treated with the ablative regimen exhibited higher activation measurements than the CDN NPs delivery to RAW cells alone (Figure 4B,C). To investigate if these

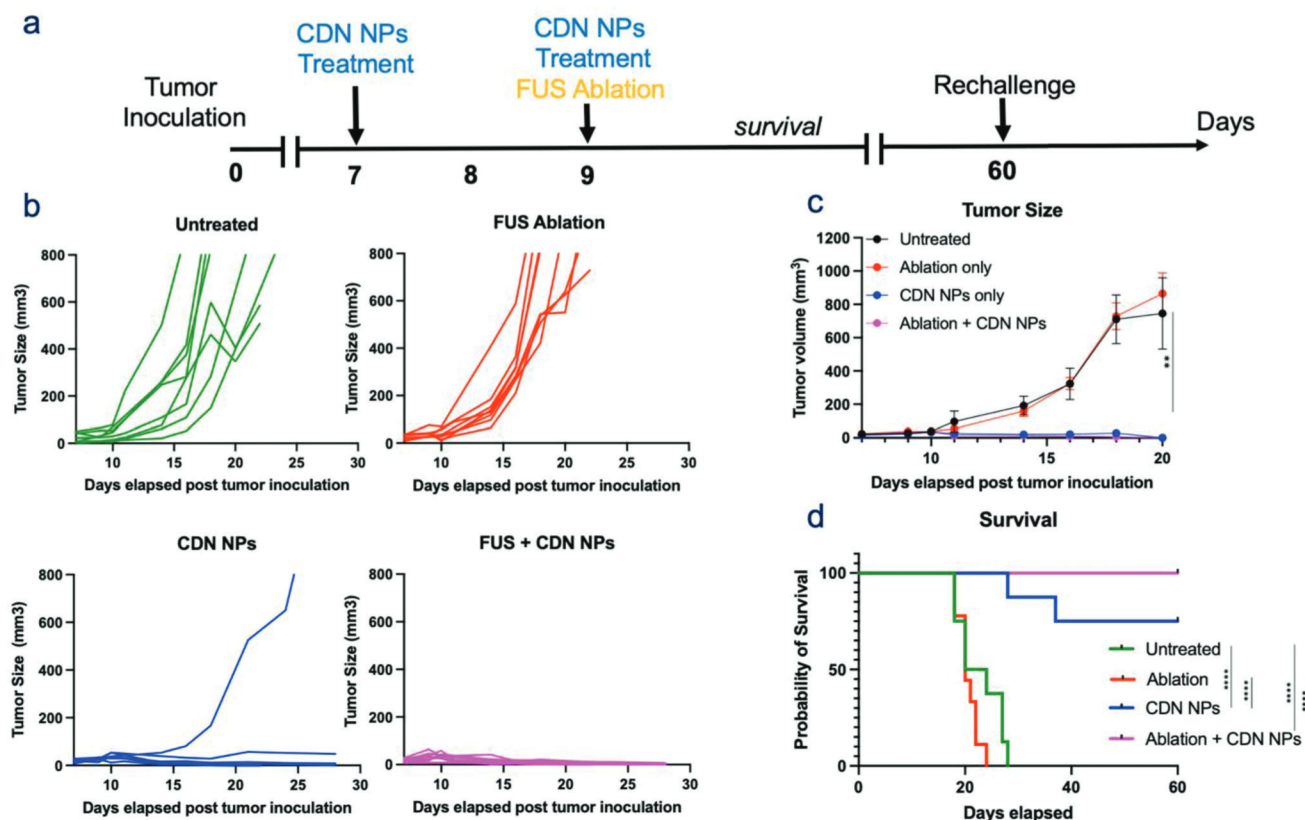


Figure 3. Treatment efficacy of CDN NPs and FUS-mediated thermal ablation. A) Treatment schedule comprised CDN NPs treatment at days 7 and 9 post-tumor inoculation as well as FUS-mediated thermal ablation on day 9. B) Individual tumor size curves following the first treatment. C) pooled tumor size curves for untreated (0/8), thermal ablation alone (0/8), CDN NPs alone (6/8), and thermal ablation + CDN NPs (9/9); Data are presented as mean \pm SEM.

effects could be detected *in vivo*, we conducted a study in which tumor-bearing mice were treated with each therapy and then applied with microneedles atop of tumors for subsequent ISF sampling. We then measured the dynamics of cytokines/chemokines in tumors, plasma, and microneedle-collected skin interstitial fluid (ISF). Biomarker analysis was initially performed using the commercially available Legendplex multiplex assay (Antiviral Response Panel, BioLegend), a bead-based immunoassay that uses the principles of sandwich ELISAs to quantify thirteen soluble analytes relevant to our therapies, using flow cytometry (Figure 4D). This assay revealed a broad increase in proinflammatory cytokine/chemokine levels following treatment with statistically significant increases in chemoattractants MCP-1, IP-10, IL12p10, and Rantes, in particular for tumors treated with CDN NPs only and CDN NPs + Ablative treatment (Figure S15, Supporting Information), while cytokine levels of tumors treated with FUS-ablation depicted characteristic elevations in KC and IL-6 expression. The assay, however, revealed several values below the limit of detection (LOD) when analyzed using skin ISF extracted by the MNs and plasma (Figure 4E).

We therefore assessed the feasibility of using Simoa for sensitive longitudinal detection of cytokines in the context of our treatments. We developed Simoa assays for the detection of keratinocytes-derived chemokine (KC) and monocyte chemoattractant 1 (MCP-1), as these chemokines are responsible for the

recruitment of neutrophils and monocytes and were previously shown to be influenced by thermal treatment.^[69–71] While IFN- β is directly overexpressed due to STING stimulation,^[59,72] IL-6 is an acute inflammatory cytokine sensitive to both ablation^[73] and STING agonism.^[74] We therefore developed Simoa assays for these four biomarkers, significantly enhancing their detection sensitivity to the femtomolar range, resulting in Legendplex:Simoa LOD ratios of 321, 2060, 258, and 1400, for KC, MCP-1, IFN- β , and IL-6, respectively (Figure S16, Supporting Information). When comparing the readings between plasma and MNs post treatment (Figure 4F; and Figure S17, Supporting Information), we observed that MNs effectively recapitulated trends seen in plasma of animals receiving combination treatment (CDN NPs + FUS ablation) broadly exhibiting higher levels of the biomarkers studied which also reflected close relationships with their expression in tumors (Figure S15, Supporting Information). When comparing the number of samples above the detection limit of the different methods assessing the ISF collected via MNs, we observed that Legendplex immunoassay was able to detect a signal in 1/16 (6%), 2/16 (13%), 1/16 (6%), 6/16 (38%), of the samples for KC, MCP-1, IFN- β , and IL-6, respectively, while Simoa was able to accurately detect 16/16 (100%), 15/19 (79%), 13/19 (68%), and 17/19 (89%) of samples for the same cytokines, measured on the day of treatment. When analyzing the same cytokines measured 24 h following treatment,

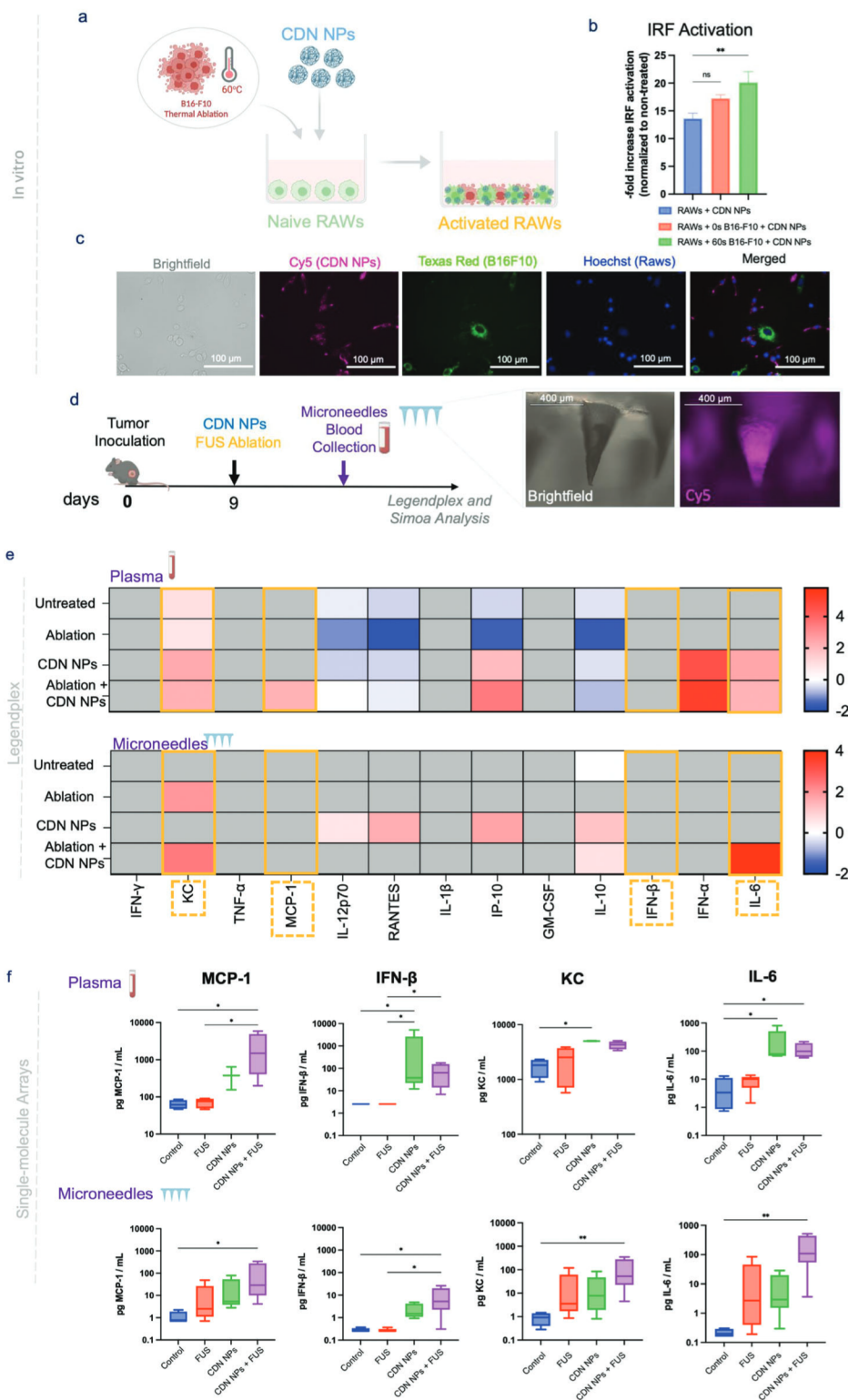


Figure 4. Thermal treatment can enhance CDN NPs immune activation, as reflected by inflammatory biomarker elevations in microneedles and plasma, sensed via Simoa. A) Treatment regimen comprising of treating B16-F10 cells with heat and immediate co-culture with RAW cells treated with CDN NPs at the same time. B) IRF activation of RAW cells cocultured with thermally treated B16F10 and CDN NPs. C) Fluorescence imaging of thermally treated B16-F10 cells (60 °C for 60 s) interacting with CDN NPs-transfected RAW cells (Cy5- CDN NPs, Hoerst—RAW nuclei). D) In vivo treatment schedule comprising of treatments: untreated, CDN NPs, FUS-mediated Ablation, and CDN NPs+ FUS Ablation. E) Heatmaps of the Legendplex-based plasma and microneedle cytokine measurements, of MNs and plasma collected 3 h post-treatment. Values below the limit of detection (LOD) are plotted in gray. F) Simoa measurements for MCP-1, IFN-β, KC, and IL-6, in plasma and MNs at the same timepoint. Data are presented as mean ± SEM.

we observed that the number of samples above the LOD were even higher for the Simoa group, of 16/16 (100%), 16/16 (100%), 16/16 (100%), and 14/18 (78%) versus 9/16 (56%), 1/16 (6%), 1/16 (6%), and 7/16 (44%) in the Legendplex method, for the same biomarkers, respectively (Figure S18, Supporting Information). Collectively, these results confirm the ultrasensitive ability of Simoa, as well as its suitability to be used in combination with MNs-ISF collection for immunotherapy monitoring.

We next investigated the effects of introducing a pretreatment with CDN NPs on day 7 prior to FUS + CDN NPs on day 9 in our efficacy study (Figure 5A). This treatment protocol was also studied in light of previous reports highlighting the positive effects of introducing immunotherapy prior to thermal ablation.^[75,76] We hypothesized that the ablation of B16-F10 cells pretreated with CDN NPs (which are major recipients of the CDN NPs in the TME) could result in high immunogenicity. To assess that, B16-F10 cells were first pretreated with CDN NPs for 48 h prior to thermal ablation and then cultured with RAW macrophages following heat treatment (Figure 5B). We found that B16-F10 cells pretreated with CDN NPs, and then treated with heat (60 s at 60 °C) elicited the most potent IRF activation levels in RAW macrophages. We observed more than 20-fold IRF increase compared to RAWs only (Figure 5C), and more than twofold increase when RAW cells were cocultured with conditioned media of B16-F10 cells pretreated with CDN NPs and then thermally ablated (Figure S19, Supporting Information). Interestingly, RAW cells cultured with ablated pretreated B16-F10 exhibited 1.6-fold higher activation than RAW cells cultured with live, not ablated pretreated with CDN NPs B16-F10 cells. Nonetheless, >15-fold higher levels of IRF activation than RAW cells alone were noted for the nonablated group (Figure 5B), likely due to phagocytosis of cancer cells and/or the transfer of CDN NPs to RAW cells as we previously demonstrated.^[59,77] Fluorescence assessment of the conditioned media of B16-F10 cells pretreated with AF647-labeled CDN NPs followed by thermal ablation, revealed increasing fluorescence levels in wells containing cells treated with heat, suggesting the likely release of cancer-cell internalized CDN NPs to the supernatant (Figure S20, Supporting Information).

We then investigated the monitoring ability of microneedles to effectively report on the immunogenicity, comparing its readings with plasma (Figure 5D). Indeed, we observed an increase in the inflammatory markers in treatment groups for both MNs and plasma, as reflected by a broad upregulation of these biomarkers for the FUS ablation + CDN NPs group, followed by CDN NPs alone, FUS, and untreated group (Figure 5E). These effects could be also observed in animals receiving CDN NPs treatment versus no treatment at day 7 (Figure S21, Supporting Information). Collectively, these results suggest that ISF sampling using noninvasive microneedle patches applied atop of treated tumors can effectively recapitulate over-time changes of cytokines/chemokines in plasma following immunotherapy treatment.

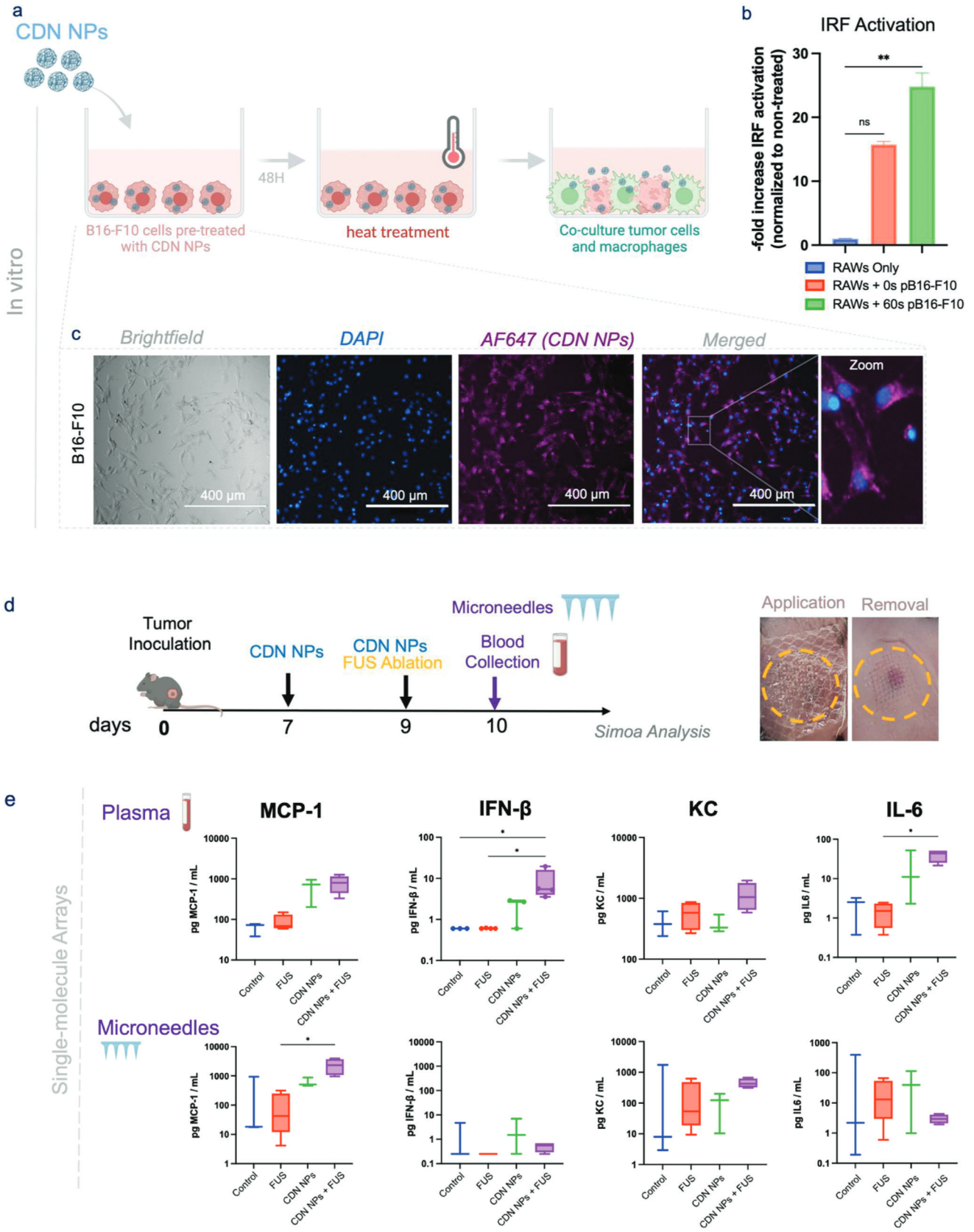
3. Discussion

More than 50% of melanoma patients do not respond to existing immunotherapies,^[4] due to primary or acquired resistance, which can arise following an initial response.^[7] Hence, the development of noninvasive methods able to longitudinally and noninvasively monitor melanoma responses to immunotherapy is

crucial for efficient patient stratification and personalization of treatments. In this study, we propose a novel monitoring strategy using polymeric microneedles for ISF sampling and ultrasensitive biomarker detection using Simoa. We used an engineered HA-based MN formulation that affords facile application, rapid swelling, and collection of biomarkers following on-demand MN degradation.

We studied the effectiveness of MN mediated ISF-biomarker sampling following tumor treatment using two model immunotherapies—STING agonism and thermal ablation. Our survival study revealed two contrasting effects for each of the therapies, with animals receiving thermal ablation exhibiting reduced survival, in contrast to CDN NPs that induced substantial tumor rejection. Interestingly, remarkable tumor rejection was observed when the therapies were combined, with a survival trend similar to that seen with CDN NPs delivery. These observations suggest that the antitumor responses noted are likely a result of STING-mediated immunity involving production of IFN-I and induction of cross-presenting DCs.^[78,79] Immunoassay profiling of tumors revealed increased IL-6 and KC expression in tumors treated with ablation only. This observation is in tandem with previous reports suggesting that without additional stimuli, DAMPs released following thermal ablation are rapidly cleared from the ablation zone, and a sterile immune response associated with wound healing phenotype arises,^[80,81] as a result of an influx of neutrophils and monocytes recruited to the site of injury and the overexpression of IL-1 β and IL-6.^[50,82–86] In the case of animals receiving CDN NPs only or with ablation, multiple proinflammatory cytokines/chemokines were upregulated with notable elevations in MCP-1, KC, RANTES, IP-10, IL-6, and IL-12p70 and GM-CSF and IFN- β , suggesting an effective proinflammatory modulation of tumors. Collectively, these observations support the argument that proinflammatory signals provided by thermal ablation can be leveraged to promote an antitumor response, especially when combined with immunomodulators, as observed in previous preclinical work,^[46,47,75,82,87,88] and is currently being investigated in clinical settings (NCT03993678, NCT04116320).

To investigate if these trends may be sensed using the proposed monitoring strategy, we next tested the ability of MNs to effectively collect ISF biomarkers under different regimens of either simultaneous FUS-ablation and STING agonism or CDN NPs serving as neoadjuvant therapy. Previous reports suggested that immune modulation prior to thermal treatment promotes an inflammatory tumor microenvironment that is able to decelerate the clearance of tumor antigens generated following thermal ablation.^[75,85,88] Both of the tested regimens exhibited potent inflammatory responses, characterized by most proinflammatory elevations in animals treated with combination treatment (FUS-ablation + CDN NPs) *in vitro* and *in vivo*, when compared to the monotherapies. We quantified biomarkers in MNs and plasma of treated animals using Legendplex, an ELISA-based immunoassays widely available and previously used as means of profiling biomarkers in the context of cancer.^[89,90] However, as the detection limit of this immunoassay was of \approx pg mL⁻¹ range and given the small volume of ISF collected (<3 μ L), we were unable to quantify biomarkers in plasma and MNs-retrieved ISF. Hence, as a proof of concept, we developed ultrasensitive Simoa assays to measure selected biomarkers of high biological relevance to



our therapies (KC, MCP-1, IFN- β , and IL-6). Using this approach, we were able to successfully detect biomarker trends at different days in the course of the treatment, which were correlated to their plasma measurements as a function of treatment, with measured limit of detection levels in the fg mL⁻¹ range. For example, MNs were able to effectively sense a spike in IFN- β expression shortly after CDN NPs administration in the groups receiving NPs intratumoral injection (Figure 4F), which returned to baseline levels 24 h later (Figure S17B, Supporting Information), a potential prognostic effect of therapy efficacy as we and others have observed in the past.^[91–93]

To date, multiple methods have been proposed with predictive or prognostic value in the context of immunotherapy monitoring. These include the measurement of biomarkers such as mutational load or PD-L1 expression, plasma analysis of cells,^[94,95] tumor exosomes,^[15,96] and biomarkers such as soluble PD-L1 (sPD-L1),^[97,98] S100B and LDH,^[10] ctDNA, cfRNA, and cmiRNA,^[15,16] cytokines,^[99] molecular imaging techniques studying growth and response of tumors,^[100,101] and microbiota analysis.^[102,103] While these methods provide clinically significant information in the context of patient stratification, their clinical adoption may be suboptimal due to their invasive nature, associated costs, and the low sensitivity for biomarkers that are diluted in the circulating blood. This study provides an additional tool for continuous monitoring of patient responses to the abovementioned arsenal of methods, by harnessing the facile application and digestion of engineered diagnostic MNs for subsequent multiplexed analysis of biomarkers via Simoa. Collecting biomarkers in a noninvasive and painless manner from the skin interstitial fluid in the vicinity of tumors may provide unique advantages, such as patient compliance, longitudinal monitoring of tumors, and higher amount of solutes sampled when compared to plasma collection. Ultimately, MNs can also be used for drug delivery applications,^[104,40] as well as for monitoring providing a theranostic platform.

Overall, our study demonstrates that melanoma immunotherapy can be monitored using polymeric microneedles, revealing the levels of relevant biomarkers that report on treatment outcomes, and correlate with those measured in the tumor and in plasma. Our results support the future use of this strategy for monitoring melanoma immunotherapy.

4. Conclusions

This study describes a monitoring strategy employing polymeric microneedles for skin interstitial fluid collection and single-molecule arrays (Simoa) for ultrasensitive protein detection, with potential to improve patient care. Our monitoring strategy confirmed the ability of biocompatible microneedles to successfully and noninvasively probe changes in biomarker profiles in ISF. These biomarkers correlate with those in plasma and tumors following treatment with model immunotherapies,

thereby serving as a reliable monitoring tool that can assist in providing personalized therapies with improved therapeutic outcomes.

5. Experimental Section

All the reagents and solvents used in this manuscript were acquired from Sigma-Aldrich unless stated otherwise. Sodium hyaluronate (60 kDa) was obtained from LifeCore Medical with a purity of at least 95%. NHS terminated 8-arm PEG was purchased from Creative PEG Works. Microneedle molds made from PDMS (11 × 11 needles with height 600 μ m, base width 300 μ m and tip to tip spacing of 600 μ m) were acquired from Blueacre Technology. Annexin V-FITC Apoptosis Detection Kit was obtained from Sigma-Aldrich. Fixable viability dye Near-IR was obtained from Thermo Fisher Scientific (MA). Antibodies against calreticulin (CRT) were obtained from Abcam (Cambridge, UK). High mobility group box-1 (HMGB1) ELISA kit was obtained from Chondrex (Washington, USA). ATP Determination Kit was obtained from Thermo Fisher Scientific (MA). Arginine peptide (H-Cys-Arg-Arg-NH₂) was obtained from CPC Scientific with a purity of more than 90%. TCDN-2 Mal was provided by Takeda Pharmaceuticals. AlexaFluor 647 (AF647) was obtained from Thermo Fisher Scientific.

Cell Lines: RAW Lucia ISG cells (InvivoGen) and murine B16-F10 and dsRed B16-F10 melanoma cells (ATCC) were maintained in Dulbecco's Modified Eagle Medium (DMEM) supplemented with 10% Fetal Bovine Serum (FBS), 2 mm L-glutamine, 25 mm (4-(2-hydroxyethyl)-1-piperazineethanesulfonic acid (HEPES), and 100 μ g mL⁻¹ penicillin, and 100 μ g mL⁻¹ streptomycin. RAW cells were also cultured with 100 μ g mL⁻¹ Normocin and Zeocin 200 μ g mL⁻¹ (InvivoGen). Cell lines were maintained in a humidified incubator at 37 °C and 5% CO₂.

CDN NPs Fabrication: CDN NPs were fabricated following the protocol fully described in Dosta et al.^[59] In brief, 25 μ L of pBAE-CR3 polymer (100 mg mL⁻¹), 20 μ L pBAE-TCDN-2 (4 mg mL⁻¹), and 5 μ L of pBAE-AF647 (2 mg mL⁻¹) were mixed resulting in conjugated TCDN2 NPs (CDN NPs). Polymer characterization was performed by dissolving in an appropriate deuterated solvent and analyzed by ¹H-NMR, recorded in a 400 MHz Varian (NMR Instruments, Clarendon Hills, IL) (Figures S1 and S2, Supporting Information). Then, 450 μ L of AcONa at 12.5 mm was added to the polymer solution and mixed. Then, following 10 min incubation at room temperature, the mixture was nanoprecipitated with 2 mL of Phosphate Buffered Saline (PBS). Finally, nanoparticle PEGylation was achieved by adding 230 μ L of NHS-PEG (2 kDa, Laysan Bio Inc.) (10 mg mL⁻¹) to the nanoparticles and reacted overnight at room temperature. The final NPs solution was purified and concentrated using centrifugal 10 kDa MWCO filters and filtered through a sterile 0.22 μ m membrane. The synthesized particles were characterized using a Zetasizer Nano ZS (Malvern Instruments, UK) which assessed size, and zeta potential. For stability, fresh particles were fabricated and size and zeta potential were acquired daily for 14 days at 4 °C.

In Vitro Evaluation of Interferon Regulatory Factor (IRF) Pathway: RAW cells were seeded in 96-well plates at 1 × 10⁵ cells per well and incubated with the different concentrations ranging from 0 to 500 nm of free CDN, CDN NPs, and CDN NPs previously heated up to 60 °C for 60 s. IRF activity was examined post-treatment using the QUANTI-Luc reagent (InvivoGen), which allows the quantification of IRF activation levels via its reaction with IRF-induced Lucia luciferase secreted into the supernatant. The experimental protocol followed the manufacturer's instructions.

Figure 5. Immunotherapy treatment prior to ablation can sustain proinflammatory signals, as reflected by biomarker elevations in microneedles and plasma, sensed via ultrasensitive Simoa. A) Treatment regimen comprising of B16F10 pretreatment with CDN NPs for 48 h (pB16-F10; 500 nm for the first 24 h followed by 50 nm for the next 24 h, and five washes with fresh media to remove free CDN NPs) followed by heat treatment and coculture with RAW cells. B) IRF activation of RAW cells cocultured with thermally treated B16F10 cells which were pre-treated with CDN NPs before ablation. C) Fluorescent images of thermally treated B16-F10 cells (60 °C for 60 s) (Texas Red) interacting with CDN NPs-transfected RAW cells (Cy5- CDN NPs, Hoerst—RAW nuclei). D) In vivo treatment schedule comprising of treatments: untreated, CDN NPs, FUS-mediated Ablation, and CDN NPs+ FUS Ablation. E) Simoa measurements for MCP-1, IFN- β , KC, and IL-6, in plasma and collected MNs; Data are presented as mean \pm SEM.

B16-F10 and RAW Cell Viability Following CDN NPs or Heat Treatment: To test the toxicity of CDN NPs, RAW cells, 96-well plates were seeded at 1×10^5 RAW cells per well and incubated with different concentrations of CDN NPs or free CDN ranging from 0 to 500 nm for 24 h. Then, cells were exposed to MTS reagent (Promega) at a concentration of 10% v/v. Cells were kept at 37 °C and absorbance was read at 490 nm. To test the effect of thermal ablation on cancer cells, Eppendorf tubes containing B16-F10 cells at a concentration of 1.5×10^5 cells mL⁻¹ were exposed to 60 °C for different durations ranging from 0 to 60 s. Heating was confirmed via temperature registration using a thermosensitive probe (IKA Works) inserted into the Eppendorf tube (Figure S3, Supporting Information). Cells were exposed to heat by introducing the containers into a digital block heater (VWR) tuned at 60 °C. Following the ablative treatment, cells were seeded in 96 well plates at a concentration of 15×10^3 cells per well and were maintained in a humidified incubator at 37 °C and 5% CO₂ for a period of 24 h. Then, cell viability was assessed using the same procedure described above.

Coculture of RAWs or Primary Macrophages, and B16-F10 Cancer Cells: Using the same heating protocol as described in the previous section, B16-F10 cell aliquots of 0.375 mL containing 5×10^5 cells were either nontreated or heated for 30 or 60 s. Following the heating treatment, the aliquots were left at room temperature for ≈ 5 min for temperature stabilization. The 0.375 mL aliquots were then treated with either free CDN or CDN NPs (1×10^6 cells mL⁻¹ and 5 nm of CDN). Then, the aliquots were added to wells preseeded for 24 h with RAW cells (24-well plate, 1×10^5 RAW cells per well). The ratio of B16-F10:RAW cells was 1:1 and final CDN concentration was 1 nm. The coculture plate was then incubated at 37 °C until the IRF activation reading of the supernatant at timepoints 24, 48, and 72 h. In some of the experiments studying the effect of CDN NPs pretreatment on B16-F10 cells, B16-F10 cells were pretreated with CDN NPs before the ablative treatment. In these experiments, during the first 24 h of CDN NPs treatment, a B16-F10 flask was treated with CDN NPs at 500 nm. Then, between 24 and 48 h the CDN NPs concentration was reduced to 50 nm (1:10 dilution with fresh media) to account for the in vivo scenario where the intratumoral concentration of drugs decays over time.^[63] Finally, before starting the heating process for pretreated B16-F10 cells, five washes with fresh media were performed in order to remove non-transfected CDN NPs. Additionally, the inhibitory effect of different ratios of RAW: B16-F10 cells treated with CDN NPs was investigated. In these experiments, a similar protocol as described above was adopted for reading the IRF activation, comparing cultures of RAW cells alone to cocultures of the two cell lines (1:5, 1:3, 1:2, and 1:1 ratios). For experiments involving primary macrophages, the cells were collected as previously described,^[59] washed, and cocultured at a ratio of 1:1 with B16-F10 cells. Cells were then stained, fixed, and analyzed by flow cytometry.

DAMP Expression Assays: For quantifying the secretion of HMGB-1 and ATP into the supernatant following heat treatment, containers with 1.15×10^6 B16-F10 cells mL⁻¹ were treated and cells were seeded in 6 well plates at a density of 3.5×10^5 cells per well and left 24 h at 37 °C. Then, the supernatant was used for determining the ATP content released into the supernatant using the ATP Determination Kit manufacturer's instruction. The supernatants were stored in -80 °C until used for HMGB-1 quantification by ELISA, using the manufacturer's instructions. To quantify calreticulin expression by B16-F10 cells following heat treatment, cells were treated at a concentration of 1.2×10^6 mL⁻¹ and seeded in 6-well plates at a concentration of 6×10^5 cells per well. Cells were incubated for 24 h at 37 °C. Next, cells were prepared for flow cytometric analysis of calreticulin expression following the manufacturer protocol. In brief, live cells were first collected by discarding the supernatant and trypsinization of the adherent cells. Then, DMEM was added to the solution and cells were washed twice with cell staining buffer and transferred to a 96 well plate. Next, Fc blocking antibodies (CD16/CD32 TruStain X, Biolegend) were added to the pellets and incubated for 5–10 min on ice. In the following, cells were washed with cell staining buffer (Biolegend) and stained by resuspending the pellets in a master mix solution containing anti-CRT (AF647, Thermo Fisher) antibodies and aqua fixable viability dye (Thermo Fisher). Cells were left in the dark, at 4 °C for 30 min. Then, cells were washed with CSB twice and resuspended in fixation buffer (Biolegend) for

10 min. Finally, cells were washed twice in CSB and stored in the dark at 4 °C, until flow cytometric analysis in the following day.

Apoptosis Assay: The state of cells was determined using an Annexin V kit and fixable viability dye near-IR (Thermo Fisher, 720/780 nm). Briefly, 24 h postheat treatment, cells were detached from wells and washed cell staining buffer twice. Next cells were washed and resuspended in $1 \times$ calcium-rich binding buffer and then 7×10^5 cells from each group were stained with Annexin V. Cells were kept in room temperature for 15 min in the dark. Cells were then washed 3x and fixed using 1% PFA diluted in binding buffer for 15 min, then washed twice with binding buffer. Cells were left in the dark overnight at 4 °C until flow cytometric analysis in the next day. The stained cells were read using Fortessa HTS II equipment and data analyzed using FlowJo Software and quantified as percentage of living (Annexin⁻/PI⁻), primary necrotic (Annexin⁻/PI⁺), apoptotic (Annexin⁺/PI⁻), and secondary necrotic cells (Annexin⁺/PI⁺).

Microneedle Synthesis: The same protocol for MNs synthesis described previously^[39] was implemented. Briefly, chemically activated 60 kDa-sodium hyaluronate (1% w/v in MES buffer) with *N*-(3-(dimethylamino)propyl)carbodiimide (EDC) and *N*-hydroxysuccinimide (NHS) (1:4:2 molar ratio) was added to a Cysteamine Dihydrochloride solution at 1:10 molar ratio, and was left reacting at room temperature for 12 h. Next, purification of HA-SS-NH₂ was performed using continuous dialysis for 6 days at room temperature. Then, purified HA-SS-NH₂ was freeze dried, and stored at -20 °C until further use (Figure S4, Supporting Information). Specially designed molds containing an 11 × 11 array of negative projections, of height of 600 μm and a radius of 150 μm were used for microneedle fabrication. The first step comprised of casting HA-SS-NH₂ polymer 10% w/v in PB, pH of 7.4, on top of the molds and centrifuged at 4200 rpm for 5 min. Then, molds were freeze dried following polymer excess removal. Next, the same procedure was repeated but this time using 8-arm-PEG-NHS 10% w/v in phosphate buffer, pH = 7.4 applied on top of the molds containing a dried layer of HA-SS-NHS. Then, a PLGA (Resomer RG 858 S, Sigma-Aldrich, USA) back layer at 15% w/v was prepared by dissolving PLGA in acetonitrile and then added dropwise to the molds until saturating the molds surface area. Microneedles were left at room temperature for ≈ 24 h until removal from molds and subsequent storage at room temperature until use.

Animal Experiments: Female, 6–8 weeks C57BL/6J mice were purchased from the Jackson Laboratory (Bar Harbour, ME) and housed in sterile conditions at the Brigham and Women's Hospital animal facility. All animal work was approved by the Institutional Animal Care and Use Committee of Brigham and Women's Hospital.

Tumor Inoculation and Experimental Protocol: While anesthetized using 2–3% isofluorane, the right flank of mice was shaved using an approved depilatory cream. Next, 5×10^5 B16-F10 cells in a volume of 50 μL were injected intradermally. Animals were then monitored 3 x week for the assessment of tumor growth via caliper measurement (calculated tumor volume = width × length × height × π/6). Tumor-bearing animals received two treatments, on days 7 and 9 post-tumor inoculation. On day 7, animals were anesthetized with 2–3% isofluorane and received CDN NPs intratumoral (I.T.) injections of 0.25 or 0.06 125 μg of CDN in a 25 μL volume. On day 9, animals received an acoustic ablative treatment immediately prior to the second I.T. injection of CDN NPs. Immediately after treatment, all treated and control animals received an application of MN, taped on top of the tumor region. The MNs were collected at different timepoints postapplication and used for cytokine collection, as described in the following.

Focused Ultrasound Ablation: The experimental setup used for heat treatment employed a FUS comprising of a 1 MHz ultrasound probe (1 cm² area, Mettler Electronics) coupled with a specially dedicated acoustic lens (focal distance = 4 mm). The FUS transducer was attached to a stereotaxic apparatus (Stoelting) platform to accurately treat distinct tumor regions. The whole observable tumor was treated by performing a raster scan in which every target received 30 s ablation and was distanced 2 mm apart from the next target in any x-y direction. Treatment was applied using CW transmission at $I = 5.1$ W cm⁻² and each tumor was treated either with 3 targets (total duration of 1.5 min) or 16 ablation spots (total duration of 8 min). For assessing the temperature elevation in the tumor, a

thermosensitive probe (Stoelting) was used for measuring the tumor temperatures during the acoustic treatment (max temperature achieved = 59 ± 1 °C).

Microneedle, Plasma, and Tumor Processing: MNs patches collected from animals were immediately incubated in containers with 200 μ L 0.1% w/v BSA, on ice. Then, the solutions were centrifuged at 10 000 rpm, 4 °C for 10 min. The supernatant was collected and stored at -80 °C for subsequent analysis using singular molecular assays (Simoa). Blood was collected using heparinized tubes via cheek bleed procedure. The collected blood was centrifuged at 10 000 rpm, 4 °C for 10 min and plasma was stored at -80 °C until used for analysis by Simoa, or Legendplex (Biolegend), using the manufacturer's protocol. Tumor tissues were collected and processed using lysis buffer and 1% Halt protease and phosphatase inhibitors (T-PER Reagent, Thermo Scientific, cat no. 75 810, 78 442) followed by filtration by centrifugation Corning Costar SpinX columns (10 000 rpm, 4 °C, 10 min) and supernatant freezing at -80 °C. The concentration of protein within the supernatants was obtained using bicinchoninic acid assay (ThermoFisher Scientific, Waltham).

Protein Detection Using Simoa: Antimouse antibodies against MCP-1 (DueSet DY479), KC (DueSet DY453), IL-6 (DueSet DY406), and IFN- β (DueSet DY8234) were purchased from R&D systems. For each target, 100 μ g of the capture antibody was coupled to 2.7 μ m carboxylated paramagnetic beads (Quanterix) using EDC (1-ethyl-3-(3-dimethylaminopropyl) carbodiimide hydrochloride) chemistry (ThermoFisher Scientific) as previously described.^[64] Detection antibodies were purchased with a biotin modification. The Simoa assays were performed on the HD-X Analyzer (Quanterix) in an automated two-step assay as previously described.^[65] IFN- β and IL-6 were measured in singleplex assays using 125 000 antibody-coated beads and 375 000 helper beads per reaction. MCP-1 and KC were measured in a multiplex assay with 125 000 antibody-coated dye-encoded beads for each marker per reaction and 250 000 helper beads per reaction. Biotinylated detection antibodies for MCP-1 and KC were combined and diluted into one solution in Homebrew Sample/Detector Diluent at a final concentration of 1 μ g mL⁻¹ each. Biotinylated detection antibodies for IFN- β and IL-6 were diluted in Homebrew Sample/Detector Diluent 1 μ g mL⁻¹. Streptavidin- β -galactosidase (S β G) Concentrate (Quanterix) was diluted to 20 μ M in S β G Diluent (Quanterix). All samples were measured in duplicate. Average Enzyme per Bead (AEB) values were calculated by the HD-X software.

Simoa Assay Validation: Protein dropout experiments were performed to assess the possibility of measuring multiple markers in a multiplexed assay as previously described.^[66] The multiplexed MCP-1 and KC had no detectable false signals arising from cross-reactivity between the two targets (Figure S5, Supporting Information). The three Simoa assays in ISF collected by MNs were validated. ISF samples with expected high protein content were serially diluted in the sample diluent. The working dilution factor was chosen to be in the middle of the linear range (5X dilution for IL6 assay and IFN- β assay, and 10X dilution for the multiplexed MCP-1 and KC assay). Each assay was then validated using a spike-and-recovery measurement: ISF samples were diluted to the working dilution factor chosen for each assay. Two concentrations of each recombinant protein were spiked into the diluted samples, and the recovery of each assay was calculated. The recovery percentages for all assays were 75–120%.

Fluorescence Microscopy: Fluorescence microscopy (Evos FL, Thermo Fisher) was used to visually assess expression of different proteins following treatment. Depending on the fluorophore used, fixed cells were exposed to different filters, such as brightfield, Texas Red (LED 720/30, Excitation 708/75, Emission 809/81), DAPI filter (LED 720/30, Excitation 708/75, Emission 809/81), and Cy5 filter (LED 475/28, Excitation 485/26, Emission 521/27). Tumor sectioning was performed by first fixating the resected tumors with 4% PFA for 3 days and subsequent ethanol storage. Then, coronal sections (5 μ m in thickness) were sliced using a Leica CM 3050S-cryostat (Leica Microsystems Nussloch GmbH, Nussloch, Germany) collected and dried on glass slides. Slide staining started by deparaffinization and subjected to antigen retrieval using citrate buffer. Slides were then incubated with anticalreticulin antibodies at a ratio of 1:100 for 1 h following the manufacturers protocol. Then, Hersh staining was performed for nuclei visualization (1:4000). Finally, slides were

covered and immediately imaged using the lasers described above. The imaging parameters were kept constant for different groups to allow for qualitative comparison.

Statistical Analysis: All statistical analyses performed in this manuscript were performed using Graph-Pad Prism 8 (GraphPad Software) for Macintosh. For all in vitro experiments, a minimum of three biological replicates were used per condition per experiment. While pairwise comparisons were performed using Student *t*-tests, multiple comparisons among groups were determined using nonparametric one-way ANOVA (Kruskal–Wallis test). No specific pre-processing of data was performed prior to statistical analyses. Statistical differences among groups were considered significant if *p*-values were below 0.05. Illustrations displayed in this manuscript were prepared using the Biorender software.

Supporting Information

Supporting Information is available from the Wiley Online Library or from the author.

Acknowledgements

M.Z.D., A.M.C., P.D., and T.G. contributed equally to this work. The authors are grateful for the funding provided by the Technion Institute of Technology, the MIT-Israel Zuckerman STEM Fund (Grant No. 2214110), the Technion Integrated Cancer Center, and the Binational Science Fund—Prof. Rahamimoff Travelgrant. Tal Gilboa is an awardee of the Weizmann Institute of Science Women's Postdoctoral Career Development Award. Michelle Dion acknowledges support from the National Science Foundation Graduate Research Fellowship and the MIT School of Engineering Evergreen Graduate Innovation Fellowship.

Conflict of Interest

David R. Walt is a founder and equity holder in Quanterix. His interests were reviewed and are managed by BWH and Partners HealthCare in accordance with their conflict of interest policies. The other authors declare no conflict of interest.

Data Availability Statement

The data that support the findings of this study are available from the corresponding author upon reasonable request.

Keywords

focused ultrasound thermal ablation, ISF biomarkers, melanoma, microneedles, nanoparticles, Simoa, STING

Received: June 5, 2023

Revised: July 7, 2023

Published online:

[1] E. B. Hawryluk, H. Tsao, *Cold Spring Harb. Perspect. Med.* **2014**, *4*, a015388.

[2] N. H. Matthews, W.-Q. Li, A. A. Qureshi, M. A. Weinstock, E. Cho, *Cutan. Melanoma Etiol. Ther.* **2017**, *3*, <https://doi.org/10.15586/CODON.CUTANEOUSMELANOMA.2017.CH1>.

- [3] J. J. Luke, K. T. Flaherty, A. Ribas, G. V. Long, *Nat. Rev. Clin. Oncol.* **2017**, *14*, 463.
- [4] J. Larkin, V. Chiarion-Sileni, R. Gonzalez, J.-J. Grob, P. Rutkowski, C. D. Lao, C. L. Cowey, D. Schadendorf, J. Wagstaff, R. Dummer, P. F. Ferrucci, M. Smylie, D. Hogg, A. Hill, I. Márquez-Rodas, J. Haanen, M. Guidoboni, M. Maio, P. Schöffski, M. S. Carlino, C. Lebbé, G. Mcarthur, P. A. Ascierto, G. A. Daniels, G. V. Long, L. Bastholt, J. I. Rizzo, A. Balogh, A. Moshky, F. S. Hodi, et al., *N. Engl. J. Med.* **2019**, *381*, 1535.
- [5] E. Faghfuri, M. A. Faramarzi, S. Nikfar, M. Abdollahi, *Expert Rev. Anticancer Ther.* **2015**, *15*, 981.
- [6] S. Maleki Vareki, *J. Immuno Therapy Cancer* **2018**, *6*, 157.
- [7] C. M. Fares, E. M. Van Allen, C. G. Drake, J. P. Allison, S. Hu-Lieskovan, *Am. Soc. Clin. Oncol. Educ. Book* **2019**, *39*, 147.
- [8] A. Tarhini, R. R. Kudchadkar, *Cancer Treat. Rev.* **2018**, *71*, 8.
- [9] W. Wang, Z. Gao, L. Wang, J. Li, J. Yu, S. Han, X. Meng, *Cancer Manage. Res.* **2020**, *12*, 9389.
- [10] S. Van Wilpe, R. Koornstra, M. Den Brok, J. W. De Groot, C. Blank, J. De Vries, W. Gerritsen, N. Mehra, *Oncoimmunology* **2020**, *9*, 1731942.
- [11] A. C. Huang, M. A. Postow, R. J. Orłowski, R. Mick, B. Bensch, S. Manne, W. Xu, S. Harmon, J. R. Giles, B. Wenz, M. Adamow, D. Kuk, K. S. Panageas, C. Carrera, P. Wong, F. Quagliarello, B. Wubbenhorst, K. D'andrea, K. E. Pauken, R. S. Herati, R. P. Staupé, J. M. Schenkel, S. Mcgettigan, S. Kothari, S. M. George, R. H. Vonderheide, R. K. Amaravadi, G. C. Karakousis, L. M. Schuchter, X. Xu, et al., *Nature* **2017**, *545*, 60.
- [12] A. Dimitrakopoulou-Strauss, *Cancer Immunol. Immunother.* **2019**, *68*, 813.
- [13] A. Natarajan, A. T. Mayer, R. E. Reeves, C. M. Nagamine, S. S. Gambhir, *Mol. Imaging Biol.* **2017**, *19*, 903.
- [14] R. Tavaré, M. N. Mccracken, K. A. Zettlitz, F. B. Salazar, T. Olafsen, O. N. Witte, A. M. Wu, *J. Nucl. Med.* **2015**, *56*, 1258.
- [15] P. Kamińska, K. Buszka, M. Zabel, M. Nowicki, C. Alix-Panabières, J. Budna-Tukan, *Int. J. Mol. Sci.* **2021**, *22*, 9714.
- [16] L. Keller, Y. Belloum, H. Wikman, K. Pantel, *Br. J. Cancer* **2021**, *124*, 345.
- [17] C. Bettgowda, M. Sausen, R. J. Leary, I. Kinde, Y. Wang, N. Agrawal, B. R. Bartlett, H. Wang, B. Lubner, R. M. Alani, E. S. Antonarakis, N. S. Azad, A. Bardelli, H. Brem, J. L. Cameron, C. C. Lee, L. A. Fecher, G. L. Gallia, P. Gibbs, D. Le, R. L. Giuntoli, M. Goggins, M. D. Hogarty, M. Holdhoff, S.-M. Hong, Y. Jiao, H. H. Juhl, J. J. Kim, G. Siravegna, D. A. Laheru, et al., *Sci. Transl. Med.* **2014**, *6*, 224ra24.
- [18] P. R. Miller, R. M. Taylor, B. Q. Tran, G. Boyd, T. Glaros, V. H. Chavez, R. Krishnakumar, A. Sinha, K. Poorey, K. P. Williams, S. S. Branda, J. T. Baca, R. Polsky, *Commun. Biol.* **2018**, *1*, 173.
- [19] J. Heikenfeld, A. Jajack, B. Feldman, S. W. Granger, S. Gaitonde, G. Begtrup, B. A. Katchman, *Nat. Biotechnol.* **2019**, *37*, 407.
- [20] J. Kool, L. Reubsæet, F. Wesseldijk, R. T. Maravilha, M. W. Pinkse, C. S. D'santos, J. J. Van Hilten, F. J. Zijlstra, A. J. R. Heck, *Proteomics* **2007**, *7*, 3638.
- [21] M. Friedel, I. A. P. Thompson, G. Kasting, R. Polsky, D. Cunningham, H. T. Soh, J. Heikenfeld, *Nat. Biomed. Eng.* **2023**, <https://doi.org/10.1038/s41551-022-00998-9>.
- [22] E. Renard, *Curr. Diabetes Rev.* **2008**, *4*, 169.
- [23] L. Tang, S. J. Chang, C.-J. Chen, J.-T. Liu, *Sensors* **2020**, *20*, 6925.
- [24] Tumor interstitial fluid: misconsidered component of the internal milieu of a solid tumor. | Semantic Scholar. <https://www.semanticscholar.org/paper/Tumor-interstitial-fluid%3A-misconsidered-component-a-Freitas-Baronzio/e1ba46ab3c212ea3ab53fb66f0709ff14ec83b05> (accessed: 30th June 2022).
- [25] H. Wiig, O. Tenstad, P. O. Iversen, R. Kalluri, R. Bjerkvig, *Fibrog. Tissue Repair* **2010**, *3*, 12.
- [26] P. G. Agache, P. Humbert, *Measuring The Skin: Non-Invasive Investigations, Physiology, Normal Constants*, Springer, Berlin **2011**.
- [27] H. Haslene-Hox, E. Oveland, K. C. Berg, O. Kolmannskog, K. Woie, H. B. Salvesen, O. Tenstad, H. Wiig, *PLoS One* **2011**, *6*, e19217.
- [28] C. Matas-Nadal, J. J. Bech-Serra, M. Guasch-Vallés, J. M. Fernández-Armenteros, C. Barceló, J. M. Casanova, C. De La Torre Gómez, R. Aguayo Ortiz, E. Garí, *J. Proteome Res.* **2020**, *19*, 2598.
- [29] K. M. Vella, I. Lara-Corrales, B. K. Rai, V. Kukreti, *JAMA Dermatol.* **2020**, *156*, 1248.
- [30] U. Kiistala, *J. Invest. Dermatol.* **1968**, *50*, 129.
- [31] R. N. O. Tettey-Amlalo, I. Kanfer, M. F. Skinner, E. Benfeldt, R. K. Verbeeck, *Eur. J. Pharm. Sci.* **2009**, *36*, 219.
- [32] S. Schmidt, R. Banks, V. Kumar, K. H. Rand, H. Derendorf, *J. Clin. Pharmacol.* **2008**, *48*, 351.
- [33] B. Yang, X. Fang, J. Kong, *Adv. Funct. Mater.* **2020**, *30*, 2000591.
- [34] T. K. Giri, S. Chakrabarty, B. Ghosh, *J. Controlled Release* **2017**, *246*, 30.
- [35] P. P. Samant, M. M. Niedzwiecki, N. Raviele, V. Tran, J. Mena-Lapaix, D. I. Walker, E. I. Felner, D. P. Jones, G. W. Miller, M. R. Prausnitz, *Sci. Transl. Med.* **2020**, *12*, eaaw0285.
- [36] H. Chang, M. Zheng, X. Yu, A. Than, R. Z. Seeni, R. Kang, J. Tian, D. P. Khanh, L. Liu, P. Chen, C. Xu, *Adv. Mater.* **2017**, *29*, 1702243.
- [37] X. Jiang, P. B. Lillehoj, *Microsyst. Nanoeng.* **2020**, *6*, 96.
- [38] Z. Wang, J. Luan, A. Seth, L. Liu, M. You, P. Gupta, P. Rath, Y. Wang, S. Cao, Q. Jiang, X. Zhang, R. Gupta, Q. Zhou, J. J. Morrissey, E. L. Scheller, J. S. Rudra, S. Singamaneni, *Nat. Biomed. Eng.* **2021**, *5*, 64.
- [39] N. Puigmal, P. Dosta, Z. Solhjoui, K. Yatim, C. Ramírez, J. Y. Choi, J. B. Alhaddad, A. P. Cosme, J. Azzi, N. Artzi, *Adv. Funct. Mater.* **2021**, *31*.
- [40] P. Dosta, N. Puigmal, A. M. Cryer, A. L. Rodríguez, E. Scott, R. Weissleder, M. A. Miller, N. Artzi, *Theranostics* **2023**, *13*, 1.
- [41] D. J. Propper, F. R. Balkwill, *Nat. Rev. Clin. Oncol.* **2022**, *19*, 237.
- [42] D. H. Wilson, D. M. Rissin, C. W. Kan, D. R. Fournier, T. Piech, T. G. Campbell, R. E. Meyer, M. W. Fishburn, C. Cabrera, P. P. Patel, E. Frew, Y. Chen, L. Chang, E. P. Ferrell, V. Von Einem, W. Mcguigan, M. Reinhardt, H. Sayer, C. Vielsack, D. C. Duffy, *J. Lab. Autom.* **2016**, *21*, 533.
- [43] D. M. Rissin, C. W. Kan, T. G. Campbell, S. C. Howes, D. R. Fournier, L. Song, T. Piech, P. P. Patel, L. Chang, A. J. Rivnak, E. P. Ferrell, J. D. Randall, G. K. Provuncher, D. R. Walt, D. C. Duffy, *Nat. Biotechnol.* **2010**, *28*, 595.
- [44] D. Wu, M. D. Milutinovic, D. R. Walt, *Analyst* **2015**, *140*, 6277.
- [45] Y. Zhu, Z. Yang, Z. Pan, Y. Hao, C. Wang, Z. Dong, Q. Li, Y. Han, L. Tian, L. Feng, Z. Liu, *Sci. Adv.* **2022**, *8*, eabo5285.
- [46] Y. Wu, Q. Li, G. Shim, Y.-K. Oh, *J. Controlled Release* **2021**, *330*, 540.
- [47] M. Zhan, X. Yu, W. Zhao, Y. Peng, S. Peng, J. Li, L. Lu, *J. Nanobiotechnol.* **2022**, *20*, 23.
- [48] A. Amouzegar, M. Chelvanambi, J. Filderman, W. Storkus, J. Luke, *Cancers* **2021**, *13*, 2695.
- [49] I. A. S. Elhelf, H. Albahar, U. Shah, A. Oto, E. Cressman, M. Almekkawy, *Diagn. Interv. Imaging* **2018**, *99*, 349.
- [50] R. J. E. Van Den Bijgaart, D. C. Eikelenboom, M. Hoogenboom, J. J. Fütterer, M. H. Den Brok, G. J. Adema, *Cancer Immunol. Immunother.* **2017**, *66*, 247.
- [51] C. T. Curley, N. D. Sheybani, T. N. Bullock, R. J. Price, *Theranostics* **2017**, *7*, 3608.
- [52] O. Cohen-Inbar, Z. Xu, J. P. Sheehan, *J. Ther. Ultrasound* **2016**, *4*, 2.
- [53] M. Chavez, M. T. Silvestrini, E. S. Ingham, B. Z. Fite, L. M. Mahakian, S. M. Tam, A. Ilovitsh, A. M. Monjazeb, W. J. Murphy, N. E. Hubbard, R. R. Davis, C. G. Tepper, A. D. Borowsky, K. W. Ferrara, *Theranostics* **2018**, *8*, 3611.
- [54] T. Su, Y. Zhang, K. Valerie, X.-Y. Wang, S. Lin, G. Zhu, *Theranostics* **2019**, *9*, 7759.

- [55] J. Fu, D. B. Kanne, M. Leong, L. H. Glickman, S. M. Mcwhirter, E. Lemmens, K. Mechette, J. J. Leong, P. Lauer, W. Liu, K. E. Sivick, Q. Zeng, K. C. Soares, L. Zheng, D. A. Portnoy, J. J. Woodward, D. M. Pardoll, T. W. Dubensky, Y. Kim, *Sci. Transl. Med.* **2015**, *7*, 283ra52.
- [56] E. L. Dane, A. Belessiotis-Richards, C. Backlund, J. Wang, K. Hidaka, L. E. Milling, S. Bhagchandani, M. B. Melo, S. Wu, N. Li, N. Donahue, K. Ni, L. Ma, M. Okaniwa, M. M. Stevens, A. Alexander-Katz, D. J. Irvine, *Nat. Mater.* **2022**, *21*, 216; **2022**, *21*, 710.
- [57] D. Shae, K. W. Becker, P. Christov, D. S. Yun, A. K. R. Lytton-Jean, S. Sevimli, M. Ascano, M. Kelley, D. B. Johnson, J. M. Balko, J. T. Wilson, *Nat. Nanotechnol.* **2019**, *14*, 269.
- [58] L. Corrales, L. H. Glickman, S. M. Mcwhirter, D. B. Kanne, K. E. Sivick, G. E. Katibah, S.-R. Woo, E. Lemmens, T. Banda, J. J. Leong, K. Mechette, T. W. Dubensky, T. F. Gajewski, *Cell Rep.* **2015**, *11*, 1018.
- [59] P. Dosta, A. M. Cryer, M. Z. Dion, T. Shiraishi, S. P. Langston, D. Lok, J. Wang, S. Harrison, T. Hatten, M. L. Ganno, V. A. Appleman, G. M. Taboada, N. Puigmal, S. Ferber, S. Kalash, M. Prado, A. L. Rodríguez, W. S. Kamoun, A. O. Abu-Yousif, N. Artzi, *Nat. Nanotechnol.* **2023**, <https://doi.org/10.1038/s41565-023-01447-7>.
- [60] J. R. Baird, D. Friedman, B. Cottam, T. W. Dubensky, D. B. Kanne, S. Bambina, K. Bahjat, M. R. Crittenden, M. J. Gough, *Cancer Res.* **2017**, *76*, 50.
- [61] T. W. Dubensky, D. B. Kanne, M. L. Leong, *Ther. Adv. Vaccines* **2013**, *7*, 131.
- [62] D. Shae, K. W. Becker, P. Christov, D. S. Yun, A. K. R. Lytton-Jean, S. Sevimli, M. Ascano, M. Kelley, D. B. Johnson, J. M. Balko, J. T. Wilson, *Nat. Nanotechnol.* **2019**, *14*, 269.
- [63] L. S. L. Price, S. T. Stern, A. M. Deal, A. V. Kabanov, W. C. Zamboni, *Sci. Adv.* **2020**, *6*, eaay9249.
- [64] M. Norman, T. Gilboa, D. R. Walt, *Clin. Chem.* **2022**, *68*, 431.
- [65] T. Gilboa, L. Cohen, C.-A. Cheng, R. Lazarovits, A. Uwamanzu-Nna, I. Han, K. Griswold, N. Barry, D. B. Thompson, R. E. Kohman, A. E. Woolley, E. W. Karlson, D. R. Walt, *Angew. Chem.* **2021**, *133*, 26170.
- [66] T. Gilboa, A. M. Maley, A. F. Ogata, C. Wu, D. R. Walt, *Adv. Healthcare Mater.* **2021**, *10*, 2001111.
- [67] M.-H. Kim, W. Liu, D. L. Borjesson, F.-R. E. Curry, L. S. Miller, A. L. Cheung, F.-T. Liu, R. R. Isseroff, S. I. Simon, *J. Invest. Dermatol.* **2008**, *128*, 1812.
- [68] Z. Lateef, G. Stuart, N. Jones, A. Mercer, S. Fleming, L. Wise, *Int. J. Mol. Sci.* **2019**, *20*, 538.
- [69] J. Shen, J. Hao, Y. Chen, H. Liu, J. Wu, B. Hu, Y. Wang, Y. Zheng, X. Cai, *J. Nanobiotechnol.* **2021**, *19*, 345.
- [70] M. G. Schwacha, B. M. Thobe, T. Daniel, W. J. Hubbard, *J. Surg. Res.* **2010**, *158*, 112.
- [71] K. Furukawa, M. Kobayashi, D. N. Herndon, R. B. Pollard, F. Suzuki, *Ann. Surg.* **2002**, *236*, 112.
- [72] J. Fu, D. B. Kanne, M. Leong, L. H. Glickman, S. M. Mcwhirter, E. Lemmens, K. Mechette, J. J. Leong, P. Lauer, W. Liu, K. E. Sivick, Q. Zeng, K. C. Soares, L. Zheng, D. A. Portnoy, J. J. Woodward, D. M. Pardoll, T. W. Dubensky, Y. Kim, *Sci. Transl. Med.* **2015**, *7*, 283ra52.
- [73] K. F. Chu, D. E. Dupuy, *Nat. Rev. Cancer* **2014**, *14*, 199.
- [74] A. H. Zaidi, R. J. Kelly, A. Gorbunova, A. N. Omstead, M. S. Salvitti, P. Zheng, J. E. Kosovec, S. Lee, S. Ayazi, L. Babar, G. G. Finley, A. Goel, B. A. Jobe, *OncoTargets Ther.* **2021**, *12*, 292.
- [75] M. T. Silvestrini, E. S. Ingham, L. M. Mahakian, A. Kheirloomoom, Y. Liu, B. Z. Fite, S. M. Tam, S. T. Tucci, K. D. Watson, A. W. Wong, A. M. Monjazebe, N. E. Hubbard, W. J. Murphy, A. D. Borowsky, K. W. Ferrara, *JCI Insight* **2017**, *2*, e90521.
- [76] N. D. Sheybani, A. R. Witter, E. A. Thim, H. Yagita, T. N. J. Bullock, R. J. Price, *J. Immunother. Cancer* **2020**, *8*, e001008.
- [77] L. Schadt, C. Sparano, N. A. Schweiger, K. Silina, V. Ceconi, G. Lucchiari, H. Yagita, E. Guggisberg, S. Saba, Z. Nascakova, W. Barchet, M. Van Den Broek, *Cell Rep.* **2019**, *29*, 1236.e7.
- [78] L. Zitvogel, L. Galluzzi, O. Kepp, M. J. Smyth, G. Kroemer, *Nat. Rev. Immunol.* **2015**, *15*, 405.
- [79] L. Zhou, Y. Zhang, Y. Wang, M. Zhang, W. Sun, T. Dai, A. Wang, X. Wu, S. Zhang, S. Wang, F. Zhou, *Adv. Biosyst.* **2020**, *4*, 1.
- [80] B. Z. Fite, J. Wang, A. J. Kare, A. Ilovitsh, M. Chavez, T. Ilovitsh, N. Zhang, W. Chen, E. Robinson, H. Zhang, A. Kheirloomoom, M. T. Silvestrini, E. S. Ingham, L. M. Mahakian, S. M. Tam, R. R. Davis, C. G. Tepper, A. D. Borowsky, K. W. Ferrara, *Sci. Rep.* **2021**, *11*, 927.
- [81] N. D. Sheybani, A. R. Witter, E. A. Thim, H. Yagita, T. N. J. Bullock, R. J. Price, *J. Immunother. Cancer* **2020**, *8*, e001008.
- [82] S. P. Haen, P. L. Pereira, H. R. Salih, H.-G. Rammensee, C. Gouttefangeas, *Clin. Dev. Immunol.* **2011**, *2011*, 160250.
- [83] V.-K.-A. Arthanareeswaran, M. Berndt-Paetz, R. Ganzer, J.-U. Stolzenburg, A. Ravichandran-Chandra, A. Glasow, J. Neuhaus, *Laparosc. Endosc. Robot. Surg.* **2018**, *1*, 5.
- [84] I. Kaplanov, Y. Carmi, R. Kornetsky, A. Shemesh, G. V. Shurin, M. R. Shurin, C. A. Dinarello, E. Voronov, R. N. Apte, *Proc. Natl. Acad. Sci. USA* **2019**, *116*, 1361.
- [85] B. Z. Fite, J. Wang, A. J. Kare, A. Ilovitsh, M. Chavez, T. Ilovitsh, N. Zhang, W. Chen, E. Robinson, H. Zhang, A. Kheirloomoom, M. T. Silvestrini, E. S. Ingham, L. M. Mahakian, S. M. Tam, R. R. Davis, C. G. Tepper, A. D. Borowsky, K. W. Ferrara, *Sci. Rep.* **2021**, *11*, 927.
- [86] B. E. Bulvik, N. Rozenblum, S. Gourevich, M. Ahmed, A. V. Andriyanov, E. Galun, S. N. Goldberg, *Radiology* **2016**, *280*, 413.
- [87] N. D. Sheybani, A. R. Witter, E. A. Thim, H. Yagita, T. N. J. Bullock, R. J. Price, *J. Immunother. Cancer* **2020**, *8*, e001008.
- [88] L. E. Muñoz, K. Lauber, M. Schiller, A. A. Manfredi, M. Herrmann, *Nat. Rev. Rheumatol.* **2010**, *6*, 280.
- [89] J. S. Lehmann, P. Rughwani, M. Kolenovic, S. Ji, B. Sun, *Meth. Enzymol.* **2019**, *629*, 151.
- [90] G. Harris, W. Chen, *Methods in Molecular Biology* **2019**, *1061*, 265.
- [91] M. C. Hanson, M. P. Crespo, W. Abraham, K. D. Moynihan, G. L. Szeto, S. H. Chen, M. B. Melo, S. Mueller, D. J. Irvine, *J. Clin. Invest.* **2015**, *125*, 2532.
- [92] S. K. Gandhapudi, M. Ward, J. P. C. Bush, F. Bedu-Addo, G. Conn, J. G. Woodward, *J. Immunol.* **2019**, *202*, 3524.
- [93] M. Wehbe, L. Wang-Bishop, K. W. Becker, D. Shae, J. J. Baljon, X. He, P. Christov, K. L. Boyd, J. M. Balko, J. T. Wilson, *J. Controlled Release* **2021**, *330*, 1118.
- [94] S. Rad Pour, Y. Pico De Coaña, X. M. Demorentin, J. Melief, M. Thimma, M. Wolodarski, D. Gomez-Cabrero, J. Hansson, R. Kiessling, J. Tegner, *J. Immunother. Cancer* **2021**, *9*, e002171.
- [95] J. Zaragoza, A. Caille, N. Beneton, G. Bens, F. Christiann, H. Maillard, L. Machet, *Br. J. Dermatol.* **2016**, *174*, 146.
- [96] J. Lesnik, T. Antes, J. Kim, E. Griner, L. Pedro, *Elife* **2016**, *5*, e07383.
- [97] Y. Okuma, H. Wakui, H. Utsumi, Y. Sagawa, Y. Hosomi, K. Kuwano, S. Homma, *Clin. Lung Cancer* **2018**, *19*, 410.
- [98] J. Zhou, K. M. Mahoney, A. Giobbie-Hurder, F. Zhao, S. Lee, X. Liao, S. Rodig, J. Li, X. Wu, L. H. Butterfield, M. Piesche, M. P. Manos, L. M. Eastman, G. Dranoff, G. J. Freeman, F. S. Hodi, *Cancer Immunol. Res.* **2017**, *5*, 480.
- [99] D. B. Johnson, J. M. Balko, *Clin. Cancer Res.* **2019**, *25*, 1452.
- [100] Z. Yang, F. Li, Y. Huang, N. Yin, J. Chu, Y. Ma, R. I. Pettigrew, D. J. Hamilton, D. R. Martin, Z. Li, *J. Nucl. Med.* **2022**, *63*, 1708.
- [101] N. Vladimirov, O. Perlman, *Int. J. Mol. Sci.* **2023**, *24*, 3151.
- [102] B. Routy, E. Le Chatelier, L. Derosa, C. P. M. Duong, M. T. Alou, R. Daillère, A. Fluckiger, M. Messaoudene, C. Rauber, M. P. Roberti, M. Fidelle, C. Flament, V. Poirier-Colame, P. Opolon, C. Klein, K. Iribarren, L. Mondragón, N. Jacquelot, B. Qu, G. Ferrere, C. Clémenson, L. Mezquita, J. R. Masip, C. Naltet, S. Brosseau, C. Kaderbhai, C. Richard, H. Rizvi, F. Levenez, N. Galleron, et al., *Science* **2018**, *359*, 91.
- [103] A. Sivan, L. Corrales, N. Hubert, J. B. Williams, K. Aquino-Michaels, Z. M. Earley, F. W. Benjamin, Y. Man Lei, B. Jabri, M.-L. Alegre, E. B. Chang, T. F. Gajewski, *Science* **2015**, *350*, 1084.
- [104] J. H. Jung, S. G. Jin, *J. Pharm. Invest.* **2021**, *51*, 503.